Effects of slow-pyrolysis conditions on the products yields and properties and on exergy efficiency: a comprehensive assessment for wheat straw

Gianluca Greco[1]*, Christian Di Stasi[1], Filipe Rego[2], Belén González[1], Joan J. Manyà[1]

[1] *Aragón Institute of Engineering Research (I3A), Technological College of Huesca, University of Zaragoza, crta. Cuarte s/n, Huesca E-22071, Spain.*

[2] *Energy and Bioproducts Research Institute (EBRI), Aston University, Aston Triangle, B4-7ET, Birmingham, United Kingdom (UK).*

* Corresponding author. E-mail address: greco@unizar.es.

ABSTRACT

In the present work, the effects of the peak temperature (400–550 °C), absolute pressure (0.2–0.9 MPa), gas residence time (100–200 s) and reactor atmosphere (pure N_2 or a mixture of CO_2/N_2) on the pyrolysis behavior of wheat straw pellets were investigated. A factorial design of experiments was adopted to assess the effects of the above-mentioned factors on the pyrolysis products, the exergy efficiencies related to them and to the overall process, and the heat required. The pyrolysis energy/exergy assessment is nowadays of great interest, for the scaling of the installations from lab-scale to commercial-scale. Results showed that, as expected, the peak temperature was the most influential factor on the yields and distributions of all the pyrolysis products as well as the char properties related to its potential stability and pore size distribution. However, an increased pressure enhanced the release of the gas species at the expense of the liquid products, without altering the final char yield. The char exergy efficiency was negatively affected by an increase in peak temperature, whereas its effect on the exergy efficiency of the produced gas resulted to be positive. It was also found that pressurized pyrolysis favored the exergy efficiency of the process, even at relatively high pyrolysis peak temperature. For the biomass feedstock and the range of operating conditions studied here, thermodynamic irreversibilities of the pyrolysis system were considerably lowered when the process was conducted at 550 °C, 0.9 MPa and using a mixture of CO_2 and N_2 as carrier gas at relatively short residence times.

KEYWORDS.

Wheat Straw; Slow Pyrolysis; Char; Pyrolysis Conditions; Energy and Exergy analysis.

1. Introduction

The term *char* refers to a carbon-rich, fine-grained, porous substance, produced from the thermal decomposition of biomass under oxygen-limited conditions and at relatively low temperatures [1]. It is otherwise known as biochar when obtained from plant biomasses and its use is addressed to soil applications. Nowadays, char can be used in a wide range of applications [2], such as solid fuel, reductant agent, soil amendment and as a precursor for activated carbons [3].

Among the wide range of thermochemical processes, slow pyrolysis is a promising route to produce char with relatively high yields, obtaining gas as a co-product for cogeneration use. As already stated by Mok and Antal [4], the pyrolysis process is very complex, since it comprises both endothermic (i.e., evaporation and tar formation) and exothermic (i.e., formation of char and gas) steps. Furthermore, the global amount of energy will depend on the operating conditions considered for the process. Hence, energy and exergy assessments are of great interest for scaling the process up to a commercial scale [5]. It is important to note that the energy analysis provides the amount of energy required for pyrolysis, while the exergy analysis gives information about the energy quality, since exergy accounts for the irreversibility of the process and the maximum work that can be obtained [6]. In other words, exergy shows a reverse relationship with energy sustainability: a decrease in energy quality loss corresponds to the incline of sustainability [7]. For this reason, its assessment could result to be of great relevance in order to evaluate and improve the efficiency related to the thermochemical routes of different biomasses [8].

Given the high number of variables affecting the pyrolysis process and the wide range of available biomass sources, a large variability in the char yield and properties should be expected. Therefore, one of the main challenges nowadays is to optimize the process conditions of pyrolysis in order to obtain the most appropriate char for a given application.

Peak temperature (also referred as highest treatment temperature) can be defined as the highest temperature reached during the pyrolysis process [9]. According to the general trend reported in

literature (see, for instance, Duman *et al.* [10], Di Blasi *et al.* [11], and Demirbaş [12]), the char yield decreases when the peak temperature increases, whereas the fixed-carbon content in the final char gradually rises with an increasing temperature [13].

Another process parameter widely reported in literature, which markedly affects the final char yield, is the gas residence time. An increase in the gas residence time (i.e., lower carrier gas flow rates) results in a prolonged contact between the solid and gas phases, leading to a further decomposition of the tarry vapors onto the solid carbonaceous matrix through secondary reactions such as condensation, repolymerization and thermal cracking [14]. As a consequence, the char yield increases at the expense of the bio-oil yield, as reported by Heo *et al.* [15], Akhtar and Amin [16], and Guedes *et al.* [17].

The effect of the absolute pressure on the char properties results to be very interesting to study in deep. To date, relatively few studies have focused on the effect of the absolute pressure on the char yield and its properties [18]. In particular, many authors such as Antal *et al.* [19,20], Rousset *et al.* [21], Recari *et al.* [22] and Qian *et al.* [23] reported an increase in the char and gas yields at the expense of the condensable fraction when both absolute pressure and gas residence time increased. This increase in char yield can be explained by a major role of the secondary reactions [24]. Nevertheless, some recent studies reported a negligible [25] or even negative effect [26] of the absolute pressure on the char yield. Such effect could be attributed to a certain enhancement of the steam gasification rate with the pressure, which results in a certain consumption of char. The magnitude of its influence will depend on the nature of the feedstock (since a high content in alkaline metals will further promote gasification) as well as the selected operating conditions in terms of vapor residence time, reactor configuration, and partial pressure of volatiles.

Another important parameter that can affect the pyrolysis behavior of biomass is the type of carrier gas employed to maintain the oxygen-limited/free conditions [27]. The introduction of a potentially oxidative carrier gas such as CO_2 in a pyrolysis environment is promising in terms of energy recovery

and ability to scale-up, since the flue gas generated by combustion of pyrolysis gas can be recycled into the pyrolysis process.

Keeping all the above-mentioned considerations in mind, the aim of the present study is to analyze the effects of peak temperature, absolute pressure, gas residence time and type of pyrolysis atmosphere (pure N_2 or a binary mixture of CO_2 and N_2, 60:40 v/v) on the pyrolysis behavior of wheat straw pellets in a lab-scale fixed-bed reactor. A 2-level full factorial design was adopted in order to study the true effects of the parameters, even considering the interaction effects among them (if any). In addition, energy and exergy assessments of the slow pyrolysis system were carried out in order to investigate the influence of the above-mentioned operating parameters on the thermodynamic performance. The novelty of this work lies not only in our experimental approach to simultaneously assess the effects of four operating conditions on the pyrolysis behavior and products properties, but also in the comparison of the operational efficiency (i.e., exergy balance) for several working conditions. To the best of our knowledge, only a few studies are found in literature reporting a comprehensive exergy assessment for different biomass sources at different pyrolysis temperatures [28], without considering any other process parameters (see, for instance, the excellent previous studies by Boateng *et al.* [29], Parvez *et al.* [30], and Atienza *et al.* [31]). Therefore, the present study is among the first ones to investigate the influence of the absolute pressure, which can certainly affect the pyrolysis exothermicity and, consequently, both the energy required for the pyrolysis process and its exergy efficiency.

2. Material and Methods

2.1 Biomass feedstock

Wheat straw (WS) pellets (7 mm OD and approximately 12 mm long) were used as raw feedstock for the char production. The WS pellets were manufactured without using any binder. The as-received biomass was directly pyrolyzed without any preliminary milling step, in order to improve the carbonization efficiency, with a consequent augment of the fixed-carbon content in the final char

[32]. The WS pellets were characterized by proximate analysis (performed in quadruplicate according to ASTM standards D3173 for moisture, D3174 for ash, and D3175 for volatile matter) as well as ultimate analysis, which was carried out in triplicate using a combustion elemental analyzer Leco CHN628 (Leco Corporation, USA). The high heating value (HHV) of the feedstock was estimated from the ultimate analysis using the Channiwala and Parikh correlation [33]. In addition, X-Ray Fluorescence (XRF) spectroscopy analysis (ADVANT'XP+XRF spectrometer from Thermo ARL, Switzerland) was performed in order to determine the inorganic constituents of the biomass ash.

The WS constituents were determined by leaching the biomass sample in a benzene/ethanol mixture, followed by a boiling step firstly in a NaOH solution, then in a H_2SO_4 solution. The description of the procedure is given in Appendix A.

2.2 Slow Pyrolysis process

2.2.1 Design of pyrolysis experiments

An unreplicated 2-level full factorial design was adopted to evaluate the true effects of four factors: peak temperature (400–550 °C), absolute pressure (0.2–0.9 MPa), gas residence time (100–200 s) and type of pyrolysis environment (from pure N_2 to a binary mixture of 60:40 v/v of CO_2/N_2, respectively). The heating rate and the soaking time (at the peak temperature) were kept constant approximately at 5 °C min^{-1} and 1 h, respectively. Three replicates at the center point (475 °C, 0.55 MPa, 150 s and 30:70 v/v of CO_2/N_2) were carried out to estimate both the experimental error and the overall curvature effect [34]. A special attention was paid on the analysis of the response variables related to the long-term stability of produced chars. Furthermore, the factorial design was also used to understand how the four factors could affect the evolution of the mass-loss rate along the pyrolysis process. For this purpose, the percentage of mass loss, the maximum value of the time-derivative of mass-loss (DTG_{max}), the area of the devolatilization peak ($Area_{peak}$) and the temperature at which DTG_{max} is attained (T_{max}) were considered as the main responses to be investigated. The structure of the regression model (using normalized values for factors in the range from –1 to 1) used during statistical analysis was the following:

$$\hat{y} = \beta_0 + \beta_1 T + \beta_2 P + \beta_3 \tau + \beta_4 CO_2 + \beta_{12} TP + \beta_{13} T{\cdot}\tau + \beta_{14} T{\cdot}CO_2 + \beta_{23} P{\cdot}\tau + \beta_{24} P{\cdot}CO_2 + \beta_{34} \tau{\cdot}CO_2 \quad (1)$$

where β_0, β_i, β_{ij} are the intercept, linear, and 2-way interaction coefficients, respectively. All the statistical calculations were conducted using Minitab software (v17). The estimated regression coefficients, the associated *p*-values (from *t*-tests) and the adjusted coefficients of determination (R^2_{adj}) were taken as indicators of the goodness of regression models.

2.2.2 Pyrolysis setup

Slow pyrolysis experiments were carried out in a bench-scale fixed-bed reactor, which was already described in a previous work [35]. A detailed outline of the pyrolysis plant is displayed in Fig. 1. Blank tests (i.e., empty reactor) were carried out in order to correct the thermal expansion effects (i.e., buoyancy effect). They were performed at the same ranges of peak temperature (400−550 °C) and absolute pressure (0.2–0.9 MPa) and using the same heating program than those conducted with biomass.

The temperature profiles inside the bed were measured by four thermocouples placed in two thermowells, located at the axis and at a radial distance of 35 mm from the axis, respectively. The thermocouples were placed two by two in the thermowells, at different heights from the bottom of the sample basket: 10 mm (TC_0 and TC_1) and 70 mm (TC_2 and TC_3). The proper residence time of the gas phase within the reactor (100–200 s at selected pyrolysis peak temperature and pressure values) as well as the pyrolysis environment (pure N_2 or a mixture CO_2/N_2) were guaranteed by adjusting the mass flow rates at STP conditions for both N_2 and CO_2. The real flow rate of the carrier gas within the reactor varied approximately between 1.60 and 3.30 L min^{-1}, which corresponded to gas-hourly space velocity (GHSV) values ranged from 18 to 36 h^{-1} (assuming a void-volume fraction of 0.9 for the entire reactor).

After each experiment, the char produced was collected and weighted. The glass traps and their flexible connections were weighted before and after each run to estimate the total mass of liquid

(organics + water). The pyrolysis liquid was recovered directly from the condensers without undergoing any washing step with solvents. The water content was evaluated by Karl Fischer titration, while the organic fraction was determined by difference from the total mass of liquid. The composition of the main components of the pyrolysis gas (i.e., CO_2, CO, CH_4 and H_2) was evaluated using a micro gas chromatograph (μ-GC, Agilent 490) equipped with two analytical columns: a PolarPlot U (He as carrier gas) and a Molsieve 5A (Ar as carrier gas).

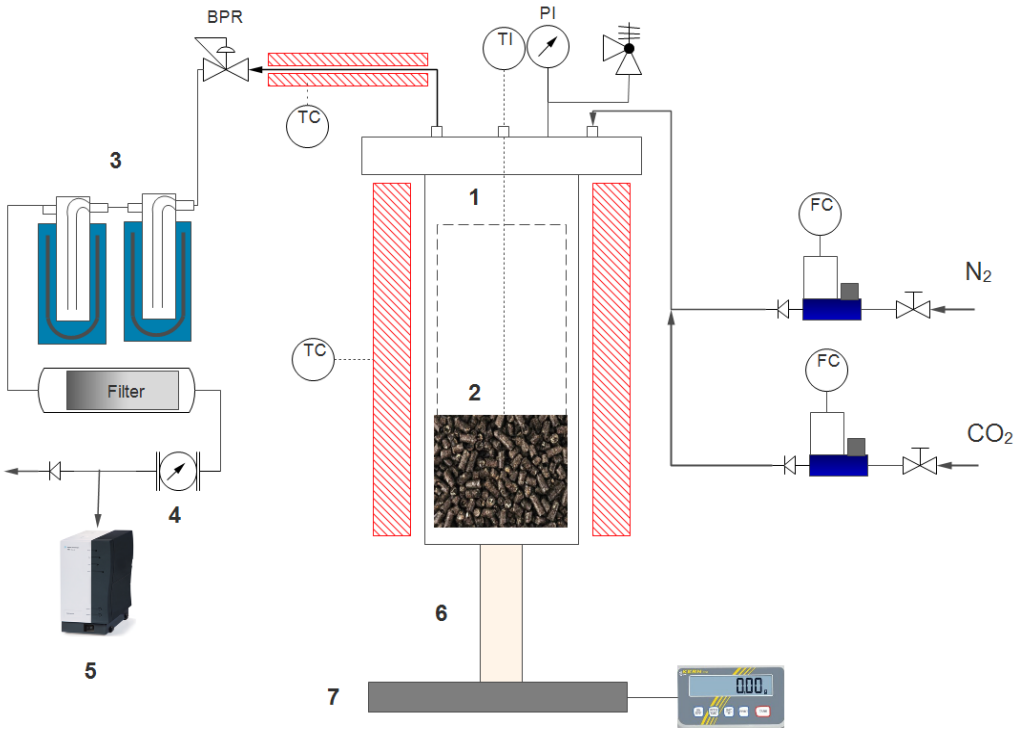

Fig. 1. Schematic layout of the pyrolysis plant: (1) pyrolysis reactor, (2) biomass bed, (3) condensation system, (4) volumetric gas meter, (5) micro-GC, (6) ceramic tube, (7) weighing platform.

2.2.3 Characterization of the pyrolysis products

The mass yield of char (y_{char}), produced gas (y_{gas}), organic condensable compounds (y_{org}) and produced water (y_{wat}) were calculated in a dry and ash-free (daf) basis. The produced char samples were characterized by proximate analysis and, additionally, ultimate analyses were performed on both chars and liquid products using the same procedures described for the biomass feedstock. The fixed-

carbon yield (y_{FC}), firstly introduced by Antal and Gronli [9], was adopted to evaluate the carbonization efficiency. It was defined as following:

$$y_{FC} = x_{FC}\, y_{char} \tag{2}$$

where x_{FC} is the fixed-carbon content in mass fraction (daf basis). The fixed-carbon yield corresponds to the fraction of organic matter initially present in the biomass feedstock, which was converted into fixed carbon.

The BET specific surface areas (S_{BET}) of the chars were determined from the CO_2 adsorption isotherms at 0 °C, since chars typically present a highly ultra-microporous structure. The adsorption isotherms were obtained using an ASAP 2020 gas sorption analyzer (Micromeritics, USA). The samples (approximately 120 mg) were firstly degassed under dynamic conditions at 150 °C until constant weight was reached. Ultra-micropore volume (V_{ultra}, i.e. pore size lower than 0.7 nm) of the samples was calculated adopting a Grand Canonical Monte Carlo method (GCMC) for carbon slit-shaped pores. All the calculations related to the adsorption isotherms were carried out using the MicroActive software (Micromeritics). In addition, Fourier transform infrared analyses (FT-IR) were performed using a Perkin Elmer FT-IR Spectrometer with PIKE Technologies GladiATR and Spectrum software in order to determine the functional groups on the surface of the produced chars. The FT-IR analyses were performed at least in triplicate under a range of wavenumber of 400 to 4000 cm^{-1} with a resolution of 4 cm^{-1}, doing 16 scans for each point in order to accomplish a reliable level of accuracy.

2.2.4 Energy and exergy assessment

The enthalpy required for the process that should be supplied externally ($Q_{process}$) and the exergy efficiencies related to the char (Ψ_{char}), produced gas (Ψ_{gas}) as well as the global exergy efficiency of the process ($\Psi_{process}$) were partly calculated using the process simulation software Aspen Plus v10 (Aspentech, USA). The pyrolysis reactor was simulated as a yield reactor block, in which the WS pellets (nonconventional component) were converted into char, CO_2, CO, CH_4, H_2, water, and condensable tars. The mass flow rate of each stream was defined on the basis of the experimental data

generated in the pyrolysis device. A layout of the control volume considered for simulations is illustrated in Fig. 2, where T_0, T_p and P are the reference temperature (25 ^{0}C), pyrolysis peak temperature (which was also considered as the process temperature) and process absolute pressure, respectively.

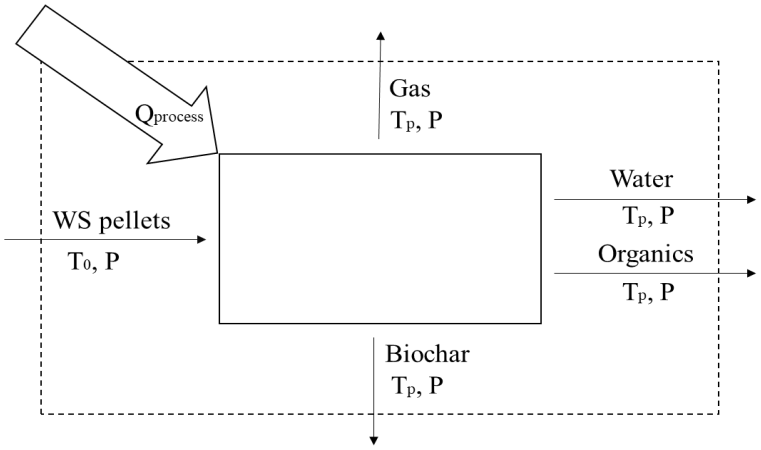

Fig. 2. A schematic layout of the control volume considered for energy and exergy assessment.

The methodology followed to calculate the energy and exergy balances was based on that reported by Atienza *et al.* [31]. Briefly, $Q_{process}$ was calculated according to Eq. (3), where h_{in} and h_{out} are the specific input and output enthalpies (in MJ kg^{-1}), respectively.

$$Q_{process}=h_{out} - h_{in} \quad (3)$$

On the other hand, the exergy efficiencies were calculated as following:

$$\Psi_i = 100\ \frac{e_{out,i}}{\Sigma e_{in}} \quad (4)$$

where $e_{out,i}$ is the exergy of the product (char or gas), and Σe_{in} is the sum of the input exergies (both physical and chemical). The exergy associated to the heat required for the process was also taken into account in Eq. (4). Calculations were conducted assuming the following considerations: (*i*) the standard reference was T_0 = 25 ^{0}C and P_0 = 0.1 MPa, (*ii*) chemical exergies for all the involved species were obtained from the literature [36], (*iii*) process heat losses as well as kinetic and potential exergies of the streams were considered to be negligible [37], (*iv*) the energy and exergy contents inherent to the carrier gas streams were considered in the respective balances, and (*v*) the exergies of condensable

tar streams were not calculated (due to the impossibility to know their real chemical composition) and thus they were taken as exergy losses.

3. Results and discussion

The full characterization of the wheat straw pellets (in terms of biomass constituents as well as proximate, ultimate and XRF analyses) is reported in Table A.1 (Appendix A). The mass-balance closures of all the pyrolysis tests were comprised between 85% and 99%. These marginal losses were attributed to errors in collecting the produced gases, especially due to the higher flow rates when the pressure increased. Therefore, the mass yields of the pyrolysis products were calculated attributing the error in the mass-balance closure to minor accuracies in determining the mass of produced gas. The repeatability of the mass-loss profiles was assessed by performing three replicates at the central point of the experimental design, which indicated a reasonable level of repeatability. Therefore, a blank test of the central point was carried out, and then subtracted to the raw mass-loss curves. Results from the analysis of repeatability are also given in Appendix A (Fig. A.1).

3.1 Pyrolysis behavior

Fig. 3 simultaneously shows the time derivative of the mass-loss and the temperature profiles, along the biomass bed at the axis (TC_0 and TC_3) and at a radial position of 35 mm (TC_1 and TC_2), for all the experiments conducted (at 400 and 550 °C, 0.2 and 0.9 MPa, and 100 and 200 s) under a pure N_2 atmosphere. As it can be seen from Fig. 3, the peak of the time derivative of the mass loss (dashed black line) was always recorded during the devolatilization step, which typically occurred between 200 and 400 °C. In this range of temperatures, exothermic peaks were visible in the temperature profiles, which are related to the heat of reaction released by the secondary reactions. According to a previous work [35], after increasing the pressure from 0.2 to 0.9 MPa, the devolatilization occurred in a narrower period of time. In other words, the devolatilization rate was higher. This was due to the effect of the absolute pressure, which greatly enhanced the kinetics of the reactions involved in the devolatilization. Also, the temperature profiles were affected by the increase in pressure, becoming

more homogeneous and reducing the gradient between them, probably due to an enhanced convective heat transfer, as a consequence of a higher N_2 flow rate to ensure the proper vapor residence time. Furthermore, the secondary charring reactions were also promoted by an increased pressure, as proved by the more pronounced exothermic peaks measured at 0.9 MPa. The observed slight decrease in temperature (of about 30 °C) after attaining the exothermic peak at higher pressures was probably due to a transient response of the PID controller (i.e., a lower power was supplied to the furnace during a relatively short period).

Interestingly, a change in the gas residence time resulted in a different shape of the devolatilization peak. As shown in Figs. 3b and 3f, after increasing the gas residence time at lower pressure (0.2 MPa), a double peak appeared. This could be due to the longer contact time between the produced tarry vapors and the forming char, leading to simultaneous production of secondary char and permanent gases. However, when the gas residence time at higher pressures increased (Figs. 3d and 3h), the double peak disappeared, similarly to what seen at low residence times (Figs. 3a, 3b, 3e and 3g). However, these peaks resulted to be lower than the corresponding peaks recorded at the same conditions of peak temperature, absolute pressure and pyrolysis atmosphere but at higher residence times. This could be explained by a combined effect of pressure and gas residence time. On the one hand, the pressure could promote devolatilization, as mentioned above, enhancing the gas production; on the other hand, an increase in pressure together with an increase in the gas residence time, can also promote the secondary charring reactions, counterbalancing the release of volatiles during the devolatilization step.

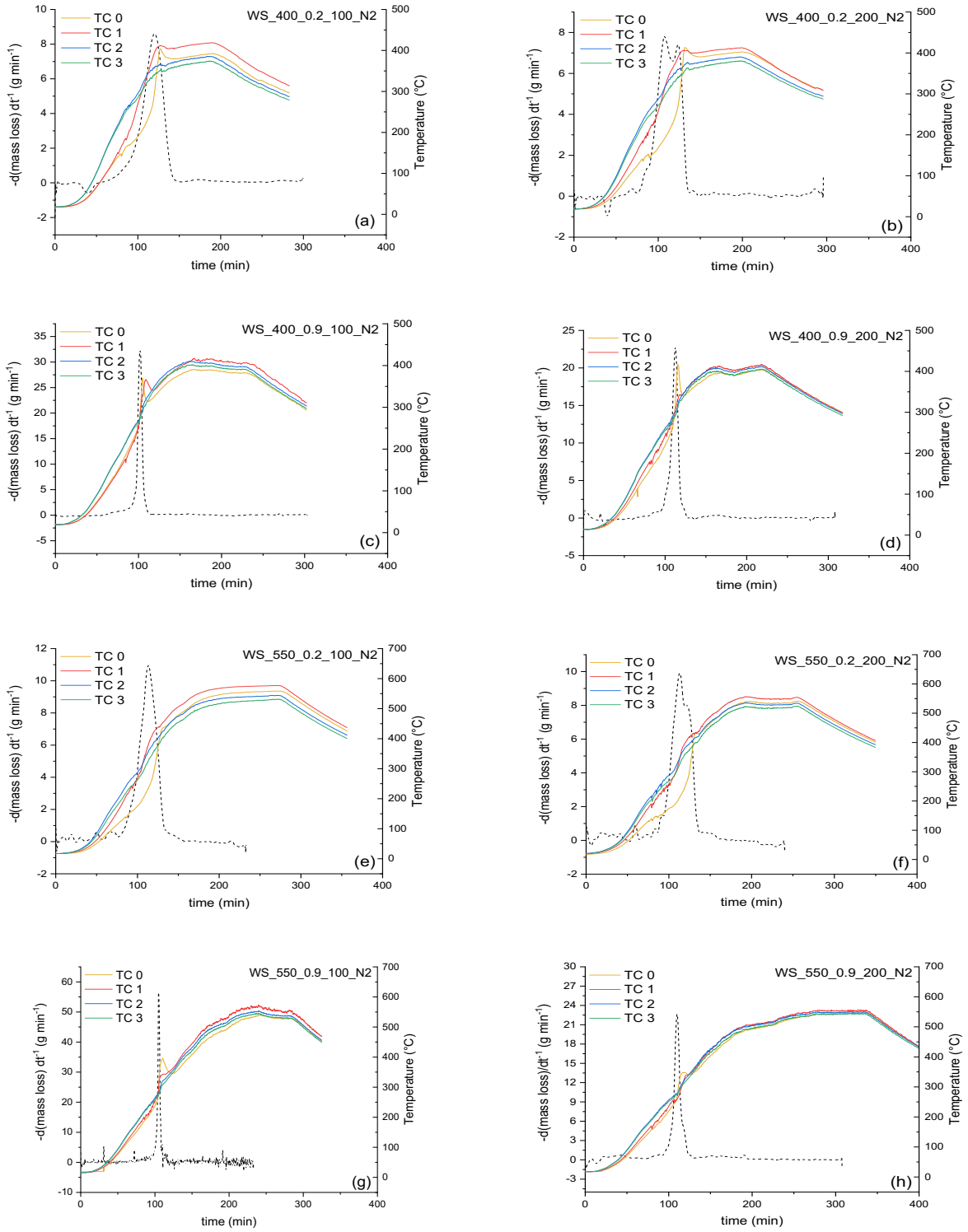

Fig. 3. Time derivative of the mass loss and evolution of the temperatures within the bed in axial (TC_0 and TC_3) and radial (TC_1 and TC_2) positions for the experiments conducted under N_2 at (a) 400 °C, 0.2 MPa and 100 s; (b) 400 °C, 0.2 MPa and 200 s; (c) 400 °C, 0.9 MPa and 100 s; (d) 400 °C, 0.9 MPa and 200 s; (e) 550 °C, 0.2 MPa and 100 s; (f) 550 °C, 0.2 MPa and 200 s; (g) 550 °C, 0.9 MPa and 100 s; and (h) 550 °C, 0.9 MPa and 200 s.

The switch from a pure N_2 atmosphere to a mixture of 60 vol. % of CO_2 and 40 vol. % of N_2 in the pyrolysis environment resulted to be irrelevant on both the evolution of the mass-loss and the temperature profiles in the entire campaign of experiments. For this reason, the plots related to the mass loss along the experiments carried out under the mixture N_2/CO_2 are not shown.

The influence of the operating conditions on the evolution of the mass-loss rate of wheat straw pellets was also investigated using the full factorial design described in Section 2.2.1. Fig. 4 displays the normal plot of the standardized effects of the operating conditions on the mass loss, T_{max}, DTG_{max} and $Area_{peak}$. As expected, the mass loss (see Fig. 4a) was favored by temperature, which promoted the thermal degradation of biomass. Furthermore, also pressure contributed to intensify the final mass loss, likely as a consequence of the relatively higher carrier flow rate, which swept the volatile species away from the reactor (thus suppressing the formation of secondary char), and, to a lesser extent, some steam gasification of char (which was promoted by the increased pressure). On the other side, an increase in the gas residence time reduced the mass loss, enhancing the secondary charring reactions, as explained above. The roles of the absolute pressure and gas residence time during the devolatilization process were confirmed from the results concerning DTG_{max} (see Fig. 4b), which resulted to be markedly enhanced by pressure and reduced when the gas residence time increased. In addition, the negative influence of the absolute pressure on $Area_{peak}$ (Fig. 4c) was completely in agreement with the observations described before (i.e., an increase in pressure results in a narrower peak). T_{max} (Fig. 4d) appeared to be positively affected by the peak temperature of the process. This could be attributed to the more severe heating when the peak temperature was higher. Furthermore, an interaction of effects between the peak temperature and the absolute pressure was responsible for a decrease in T_{max}, probably due to some convective effect related to the higher flow rate of carrier gas used at high pressure. More details about the statistics and the numerical results of this section are given in Tables A.2 and A.6.

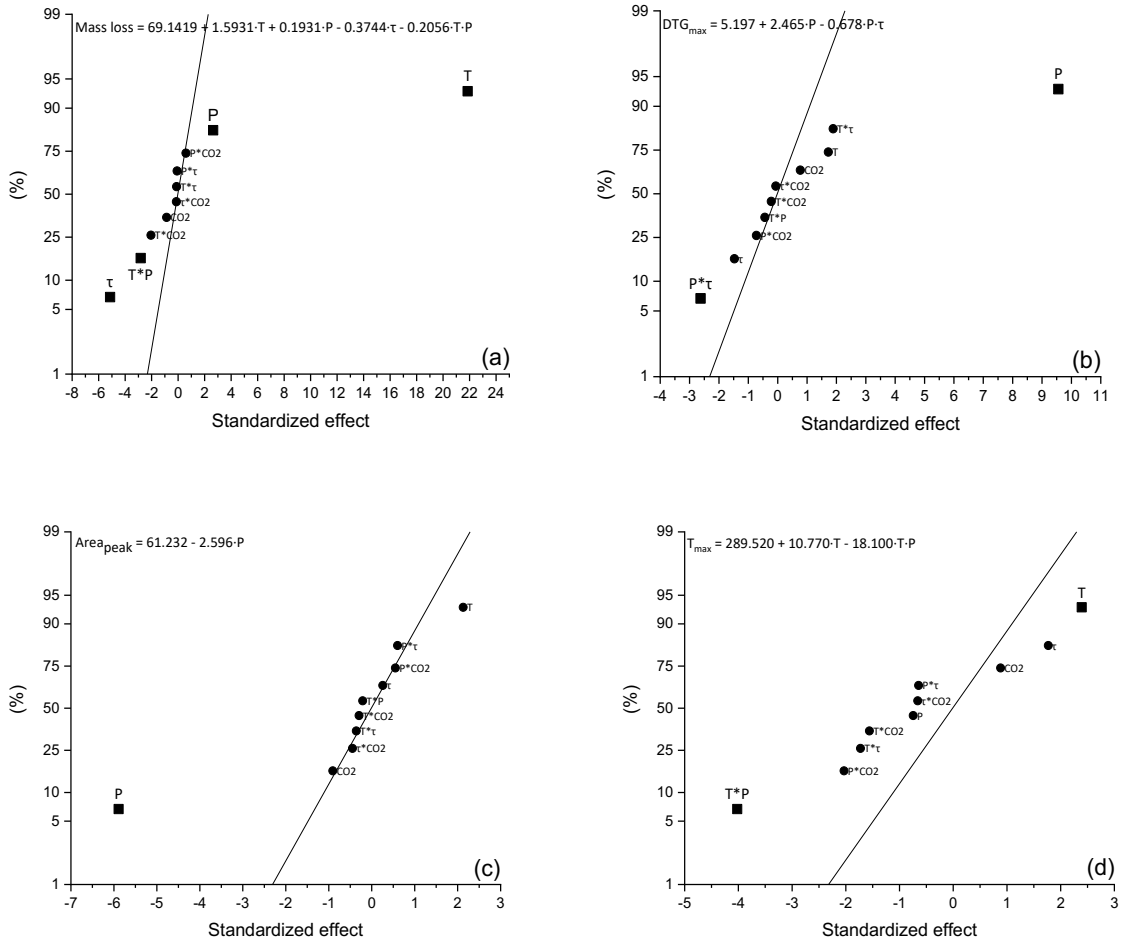

Fig. 4. Normal plots of standardized effects (α=0.05) for (a) the mass loss (%), (b) DTG_{max}, (c) $Area_{peak}$, and (d) T_{max} (square, significant effect; circle, non-significant effect). Regression models are given above each plot.

3.2 Pyrolysis products distribution

The distributions of the pyrolysis products obtained along the experiments is listed in Table 1. In the next subsections, results concerning the yield of char, condensable organic compound and permanent gases are discussed. The statistical results related to this section are given in Table A.3.

Parameter				Response variable							
T (^{0}C)	P (MPa)	τ (s)	CO_2 (%v)	y_{char} (−)	y_{org} (−)	y_{wat} (−)	y_{gas} (−)	y_{CO2}[1]	y_{CO}[1]	y_{CH4}[1]	y_{H2}[1]
550	0.2	100	0	0.276	0.084	0.307	0.334	5.365	2.917	0.215	1.333
475	0.55	150	30	0.294	0.125	0.291	0.360	5.310	3.606	0.975	0.387
550	0.9	100	0	0.276	0.105	0.207	0.413	7.099	1.877	1.939	1.546
400	0.9	100	0	0.317	0.098	0.163	0.421	7.174	3.115	0.520	0.092
400	0.2	100	0	0.311	0.133	0.240	0.316	5.037	2.896	0.457	0.057
475	0.55	150	30	0.290	0.102	0.227	0.380	3.970	3.478	0.934	0.377
550	0.2	200	60	0.288	0.111	0.290	0.311	3.881	3.694	1.431	0.942
400	0.2	100	60	0.293	0.146	0.311	0.251	3.949	2.374	0.345	0.043
400	0.9	200	0	0.324	0.094	0.199	0.383	6.543	2.637	0.636	0.105
550	0.2	100	60	0.280	0.123	0.283	0.314	2.872	5.180	1.732	1.326
550	0.2	200	0	0.285	0.112	0.268	0.335	5.176	2.690	1.371	1.133
550	0.9	100	60	0.279	0.093	0.202	0.425	7.324	3.168	0.419	0.447
400	0.9	200	60	0.317	0.096	0.190	0.397	7.562	1.787	0.515	0.070
400	0.2	200	60	0.332	0.137	0.275	0.257	3.763	2.790	0.428	0.049
475	0.55	150	30	0.297	0.101	0.238	0.364	5.427	3.391	1.026	0.421
550	0.9	200	60	0.288	0.109	0.251	0.352	5.763	2.677	0.988	0.395
400	0.2	200	0	0.327	0.122	0.265	0.286	4.699	2.363	0.410	0.043
400	0.9	100	60	0.309	0.084	0.167	0.440	7.678	2.724	0.979	0.108
550	0.9	200	0	0.284	0.085	0.216	0.414	6.832	2.465	1.770	1.574

[1] The gas yields are given in mmol g^{-1} of daf biomass.

Table 1. Experimental distributions obtained respectively for y_{char}, y_{org}, y_{wat}, y_{gas}, y_{CO2}, y_{CO}, y_{CH4} and y_{H2}.

3.2.1 Char yield

The normal plot of the standardized effects of the operating conditions on the resulting char yield is reported in Fig. 5. According to the results illustrated for the mass loss in Section 3.1, an increase in the peak temperature led to a decrease in the final char yield, whereas an increase in the gas residence time significantly improved it.

The effect of peak temperature was qualitatively in agreement with a large number of studies available in literature [11,38], which reported a higher thermal degradation of cellulose and

hemicelluloses in the range of 250–450 °C [39], depending on the type of feedstock. Moreover, the effect of the gas residence time agreed with the results obtained for the mass loss. As mentioned above, an increase in the gas residence time resulted in a prolonged contact between the gas and solid phases, allowing the tarry vapors to repolymerize with a major extent instead of leaving the reaction zone as they were produced. As a consequence, the resulting char yield was higher. In addition, the char yield did not seem to be affected by the absolute pressure, according to Melligan *et al.* [25] and to one of our previous works [35]. However, this result is also in contrast with many earlier works; for instance, Manyà *et al.* [26,40] reported in both studies a negative effect of the absolute pressure on char yield, whereas Noumi *et al.* [41] observed a decrease in char yield when pressure increased. The reasons for this discrepancy could be various, such as the range chosen for the gas residence time, which may result too short to appreciate the pure effect of the pressure on the char yield. Another possible explanation could be that the effect of pressure, responsible of the formation of the secondary char, is counterbalanced by another effect of itself, which promotes a low (but certain) extent of the steam gasification. In other words, the additional char produced through secondary charring reactions could be compensated by a certain consumption of carbon via steam gasification. This theory is strengthened by the presence of alkali and alkaline earth metal species (AAEMs) contained in the wheat straw pellets, which enhance the kinetics of the reaction under higher pressures [42]. The experimental char yields, which are reported in in Table 1, varied from 0.276 to 0.332. As expected, the lowest values were obtained from pyrolysis at 550 °C and a gas residence time of 100 s.

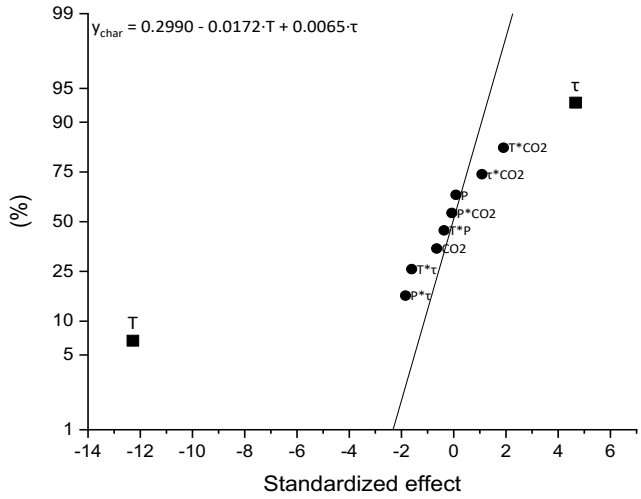

Fig. 5. Normal plot of the standardized effects (α=0.05) for y_{char} (square, significant effect; circle, non-significant effect). Regression models are given above each plot.

3.2.2 Organic condensable compounds and produced water yields

Fig. 6a shows the normal plot of the standardized effects of the selected parameters on the yield of organic condensable compounds. As expected, the absolute pressure had a remarkable, negative effect on it, since typically an increase in pressure favors the gas yield at the expense of the condensable products. In addition, the pressure promotes the formation of secondary char, leading to a higher consumption of volatiles and a further release of permanent gases (Fig. 6a). According to this, y_{org} decreased up to 0.084 (see Table 1) when pressure was high. The enhanced production of gases with high pressures also affected negatively the water yield (Fig. 6b), as already reported by Ates *et al.* [43], probably due to an enhancement of reaction kinetics such as that of the water gas shift (also thermodynamically favored at lower temperatures), which led to a higher consumption of water.

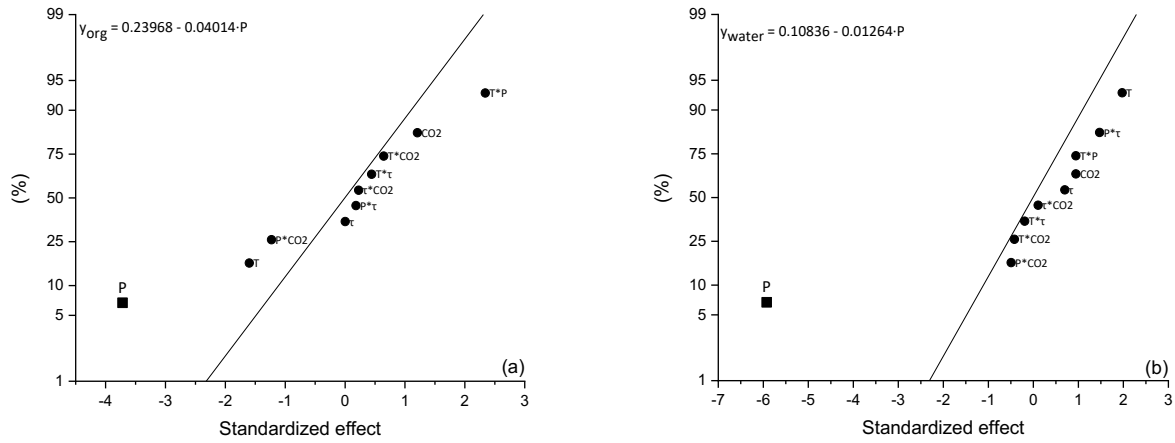

Fig. 6. Normal plots of the standardized effects (α=0.05) for (a) y_{org} and (b) y_{water} (square, significant effect; circle, non-significant effect). Regression models are given above each plot.

3.2.3 Non-condensable gases yield and their distributions

As visible in Fig. 7, the total gas yield was greatly affected by the absolute pressure, which boosted the release of gaseous species up to 0.440 (see Table 1). The yields of the main gas components (CO_2, CO, CH_4 and H_2) have been analyzed and the normal plots of the standardized effects of the operating conditions on them are displayed in Fig. 8, whereas their yields are listed in Table 1. The yield of CO_2 (Fig. 8a) markedly increased with pressure, primarily due to the promoted decarboxylation of hemicelluloses and cellulose [23]. An increase in pressure also resulted in a lower yield of CO (Fig. 8b), likely due to the promotion of the water gas shift reaction kinetics. This was completely in agreement with the considerations related to the water content described above. An additional consumption of CO could be due to a certain extent of the Boudouard reaction at high pressure. In addition, and as deduced from Fig. 8b, the Boudouard equilibrium could be shifted towards the CO production when the peak temperature and CO_2 concentration in the pyrolysis atmosphere increased, thus leading to a higher y_{CO}. Regarding the CH_4 and H_2 releases (Figs. 8c and 8d), their yields notably increased with the peak temperature, as a consequence of a major extent of the methanation and dehydrogenation reactions at temperatures above 500 °C.

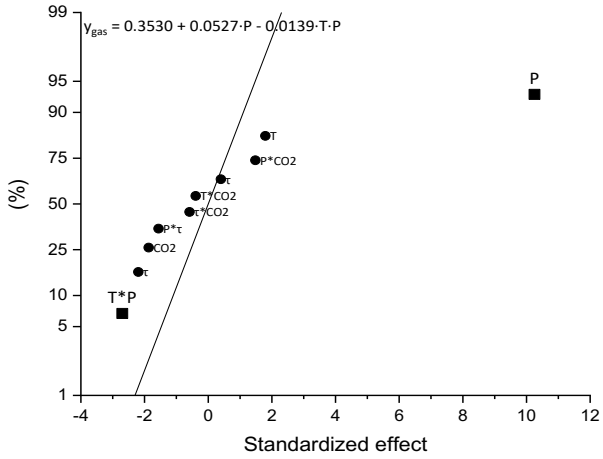

Fig. 7. Normal plots of the standardized effects (α=0.05) for y_{gas} (square, significant effect; circle, non-significant effect). Regression models are given above each plot.

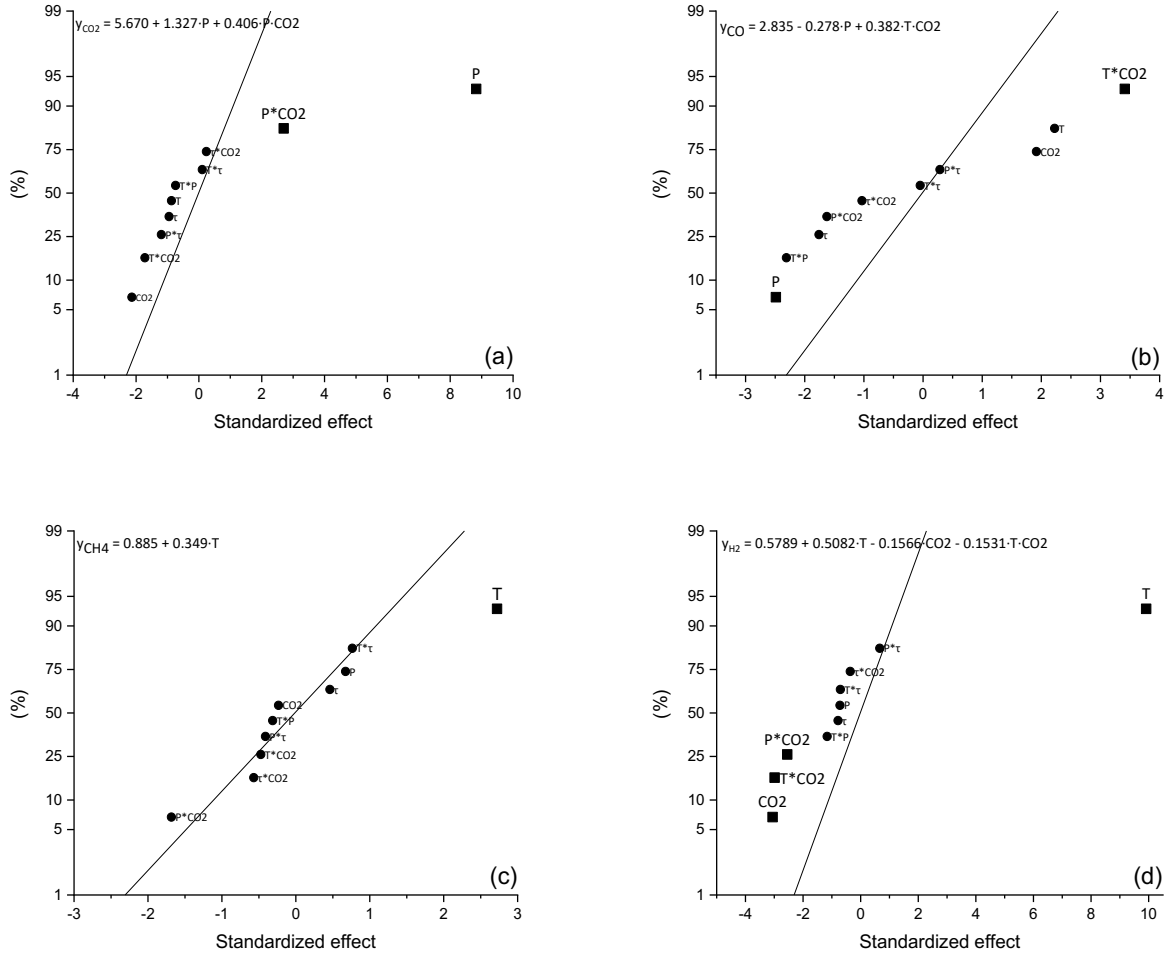

Fig. 8. Normal plots of standardized effects (α=0.05) for (a) y_{CO2}, (b) y_{CO}, (c) y_{CH4} and (d) y_{H2} (square, significant effect; circle, non-significant effect). Regression models are given above each plot.

3.3 Char properties

The char properties related to its potential stability and textural properties are shown in Table 2. All the regression coefficients of the models related to this section are shown in Table A.4.

Parameter				Response variable					
T (^{0}C)	P (MPa)	τ (s)	CO_2 (%v)	H:C (−)	O:C (−)	x_{FC} (%)	y_{FC} (−)	S_{BET} ($m^2\ g^{-1}$)	V_{ultra} ($cm^3\ g^{-1}$)
550	0.2	100	0	0.3683	0.0811	83.8538	0.230	229	0.085
475	0.55	150	30	0.4637	0.1066	81.9321	0.239	203	0.050
550	0.9	100	0	0.3527	0.0684	86.5415	0.238	214	0.080
400	0.9	100	0	0.6169	0.1125	72.5910	0.236	154	0.049
400	0.2	100	0	0.6720	0.1526	71.8470	0.220	157	0.052
475	0.55	150	30	0.4627	0.0931	80.4669	0.232	194	0.071
550	0.2	200	60	0.3650	0.0728	86.3462	0.248	217	0.081
400	0.2	100	60	0.6300	0.1357	72.9954	0.214	157	0.052
400	0.9	200	0	0.6081	0.1141	75.3153	0.243	160	0.052
550	0.2	100	60	0.3374	0.0734	86.1236	0.240	222	0.086
550	0.2	200	0	0.3662	0.0699	86.1469	0.244	216	0.082
550	0.9	100	60	0.3294	0.0679	85.5851	0.236	219	0.083
400	0.9	200	60	0.5696	0.1013	76.2568	0.242	158	0.050
400	0.2	200	60	0.6498	0.1299	72.4933	0.240	152	0.049
475	0.55	150	30	0.4739	0.0993	81.6941	0.242	187	0.067
550	0.9	200	60	0.3312	0.0633	85.8450	0.244	224	0.086
400	0.2	200	0	0.6350	0.1219	74.1738	0.242	152	0.049
400	0.9	100	60	0.5462	0.0992	76.8011	0.237	159	0.052
550	0.9	200	0	0.3422	0.0669	86.4768	0.245	213	0.082

Table 2. Experimental results of H:C and O:C atomic ratios, x_{FC}, y_{FC}, S_{BET} and V_{ultra} related to the produced chars.

3.3.1 Potential stability and aromatic fraction

The fixed carbon content and the atomic H:C and O:C ratios were considered as rough indicators of the potential stability (i.e., carbon sequestration potential) of the produced chars. In light of the results displayed in Fig. 9, it can be deduced that the potential stability was markedly improved by both the peak temperature and, to a lesser extent, absolute pressure. In fact, the increase in peak

temperature led to higher fixed carbon contents (up to 86.6%), due to the higher aromatization of the char structure, making it more stable. This is also confirmed by the reduction of both H and O contents in the char, as it could be deduced from Figs. 9b and 9c for the atomic H:C and O:C ratios, respectively. The positive effect of the absolute pressure on the char stability was a direct consequence of its role played in the production of secondary char (as mentioned in Section 3.2.1), which is less reactive and more stable than the primary one.

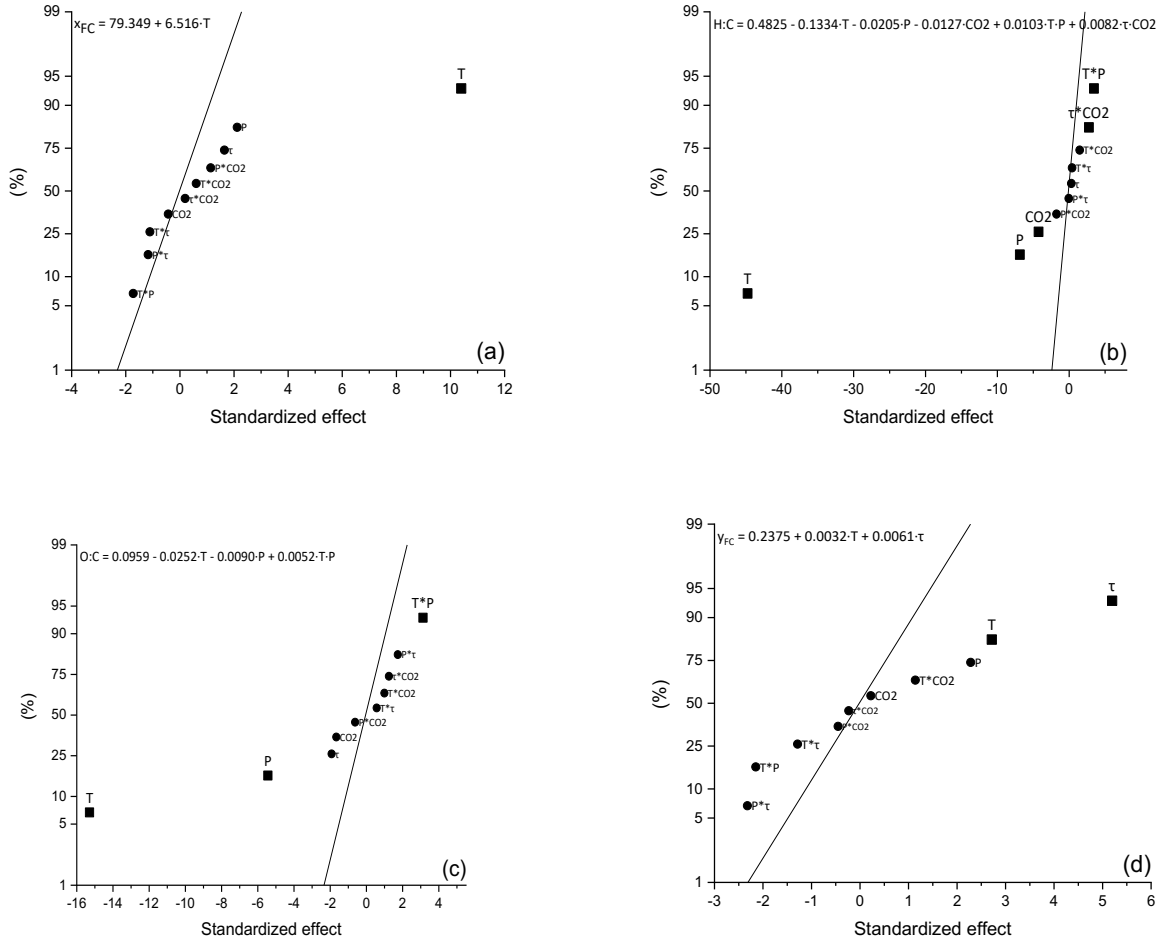

Fig. 9. Normal plots of standardized effects (α=0.05) for (a) x_{FC}, (b) atomic H:C ratio, (c) atomic O:C ratio and (d) y_{FC} (square, significant effect; circle, non-significant effect). Regression models are given above each plot.

From Fig. 9d, it can be seen that the fixed-carbon yield was positively affected by both the peak temperature and gas residence time. In particular, the effect of the latter resulted to be more significant, since the effect of the peak temperature was the product of its positive contribution to the

x_{FC} and its negative one to the y_{char}. In light of these results, it was possible to deduce that the highest value of y_{FC} was achieved for the experiments carried out at 550 °C and 200 s, with a value comprised between 0.24 and 0.25 (see Table 2).

3.3.2 Textural properties

Fig. 10 shows the normal plots of the standardized effects of the operating conditions on the BET surface area (S_{BET}) and the ultra-micropore volume (V_{ultra}). It appeared that the peak temperature was the only factor to significantly affect both the surface area and the ultra-micropore volume. This was probably due to a more extended thermal degradation of biomass at higher temperatures leading to a further release of the volatile species, thus leading to the formation of new pores. The ranges of values of S_{BET} and V_{ultra} were 152–229 m^2 g^{-1} and 0.049–0.085 cm^3 g^{-1}, respectively. Interestingly, the absolute pressure had no significant effect on the porosity development in the range of 0.2–0.9 MPa, in contrast with previous works [25,44], which reported a slight or even dramatic decrease in the BET surface area. This result was attributed to a clogging of the pores by tar deposits as a consequence of the high pressure. In this sense, the observed no significant effect of the absolute pressure on the textural properties analyzed here makes mild pressurized pyrolysis particularly attractive to produce wheat straw-derived chars with enhanced properties in terms of potential stability without affecting their porosity development.

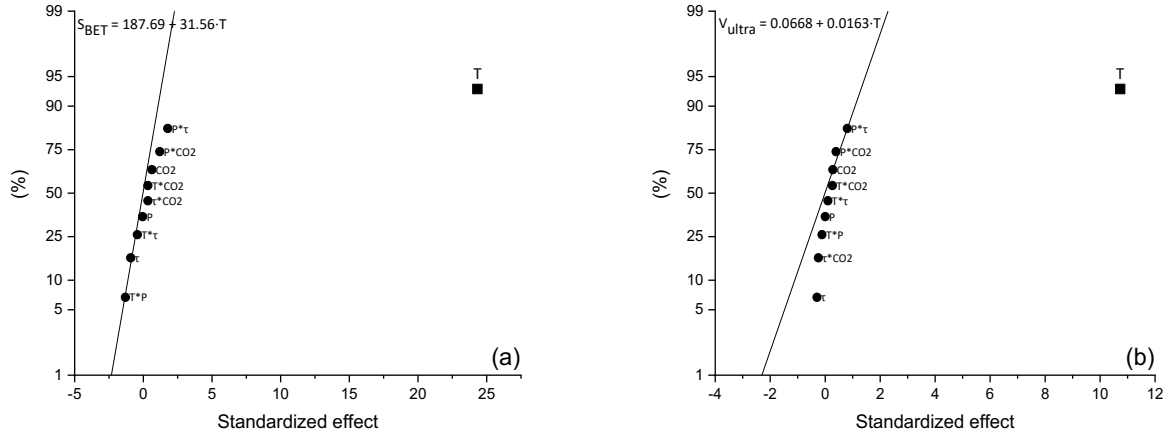

Fig. 10. Normal plots of standardized effects (α=0.05) for (a) S_{BET} and (b) V_{ultra} (square, significant effects; circle, non-significant effects). Regression models are given above each plot.

3.3.3 FT-IR Spectra and surface chemistry

Results from FT-IR spectra firstly showed that the gas residence time seemed to have no effect on the char surface chemistry. Hence, only the set of spectra for chars obtained at 200 s is shown in Fig. A.2. The switch from a pure N_2 atmosphere to the mixture CO_2/N_2 at 400 °C resulted into a slight increase in the bands at 1250, 1550 and 1750 cm^{-1}, which correspond to oxygen-containing groups, such as lactones, carboxyl groups, aldehydes and ketones. A substantial decrease in all the bands was observed when the temperature increased from 400 °C to 550 °C, as a consequence of a decrease in the volatile content and, thus, in the surface functionalities of the produced chars. The presence of CO_2 in the atmosphere at 550 °C, regardless of the pressure applied, led to higher bands visible in the spectra than those observed under a N_2 atmosphere, especially around 1250 cm^{-1} (C-O vibrations), probably due to a certain surface oxidation.

3.4 Energy and exergy analysis

Fig. 11 shows the normal plot of the standardized effects of the selected operating factors on $Q_{process}$ and the exergy efficiencies, whereas the energy and exergy balances obtained along the whole set of experiments are summarized in Table 3. The statistics outcomes related to this section are reported in Table A.5.

First, it is important to note that the most part of the $Q_{process}$ values resulted to be slightly negative, in contrast with the values typically low but positive reported in literature for pyrolysis at atmospheric pressure [45]. This could be attributed to the reactor pyrolysis configuration (in which the carrier gas is not forced to pass through the bed) as well as the relatively large particle size of WS pellets. Both factors might result in enhanced secondary reactions, which are highly exothermic.

From Fig.11a, it can be observed that a further increase in the absolute pressure from 0.2 MPa to 0.9 MPa led to higher values of $Q_{process}$. This result, which seems to be contradictory to the more exothermic peaks observed for experiments conducted at 0.9 MPa (see Fig. 3), could be explained by a dilution of the exothermicity of the overall process, due to the increase in the carrier gas flow rate

at high pressure (to guarantee the proper gas residence time), since the higher the flow rate, the higher the heat needed to be supplied to the system.

Parameter				Response variables			
T (^{0}C)	P (MPa)	τ (s)	CO_2 (%v)	$Q_{process}$ *(MJ kg^{-1})*	Ψ_{char} (%)	Ψ_{gas} (%)	$\Psi_{process}$ (%)
550	0.2	100	0	–0.50	40.94	12.27	54.94
475	0.55	150	30	–0.65	42.87	10.67	55.52
550	0.9	100	0	–0.18	40.90	16.19	58.99
400	0.9	100	0	0.01	46.70	10.32	59.55
400	0.2	100	0	–0.39	52.01	7.63	60.62
475	0.55	150	30	0.18	42.98	11.96	56.69
550	0.2	200	60	–0.48	42.93	14.55	58.91
400	0.2	100	60	–0.54	42.56	6.10	51.97
400	0.9	200	0	–0.21	48.06	9.42	59.24
550	0.2	100	60	–0.38	40.66	15.70	58.11
550	0.2	200	0	–0.53	42.65	12.74	56.59
550	0.9	100	60	0.79	41.92	14.16	59.53
400	0.9	200	60	–0.22	47.03	6.74	55.54
400	0.2	200	60	–0.32	48.45	7.26	56.92
475	0.55	150	30	–0.34	43.90	12.88	58.51
550	0.9	200	60	–0.10	43.63	10.26	55.92
400	0.2	200	0	–0.65	48.08	7.02	56.28
400	0.9	100	60	0.42	45.71	11.08	59.09
550	0.9	200	0	–0.05	42.47	16.10	60.38

Table 3. Experimental results obtained for $Q_{process}$, Ψ_{char}, Ψ_{gas} and $\Psi_{process}$.

An increase in the pyrolysis peak temperature resulted to be significantly negative for Ψ_{char} (Fig. 11b), meaning that the useful work obtained from chars produced at 550 °C was lower than that of chars produced at 400 °C. A reason to explain this finding is the lower yields of high-temperature chars. It is also important to highlight that, although the greater irreversibility, more severe conditions of temperature generally develops other important properties in the char, such as higher surface area and higher recalcitrance. In light of this, depending on the application that char addresses, it would be more or less appropriate to increase the temperature at the expense of a greater irreversibility.

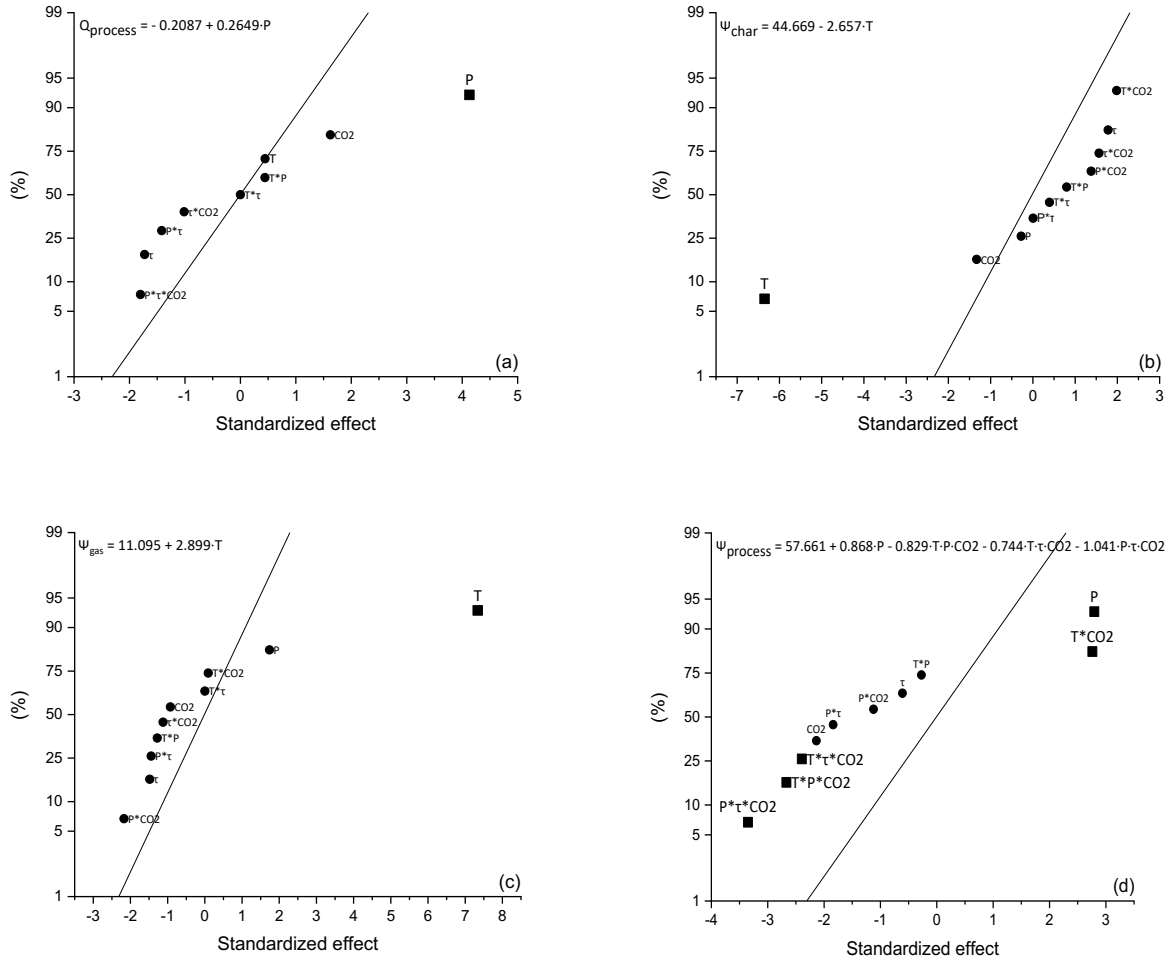

Fig. 11. Normal plots of standardized effects (α=0.05) for (a) $Q_{process}$; (b) Ψ_{char}; (c) Ψ_{gas}; and (d) $\Psi_{proccess}$ (square, significant effects; circle, non-significant effects). Regression models are given above each plot.

The peak temperature positively affected Ψ_{gas}, since more refined gas products were released at higher pyrolysis temperatures. As seen from Fig. 11d, the absolute pressure was the only factor that had a significant (and positive) main effect on the exergy efficiency of the overall process. The available literature focused on the effects of pressure on the exergy efficiency is very limited and mainly restricted to gasification processes. Nonetheless, the positive effect of pressure on the exergy efficiency was already observed by Srinivas *et al.* [46]. The opposite trend was however observed by Prins *et al.* [47] and Wang *et al.* [28], who reported a negative effect of pressure on the exergy efficiency of the overall biomass gasification process. From the regression model for $\Psi_{process}$, which

is given in Fig. 11d, it can be deduced that two sets of operating conditions (both at high pressure and peak temperature) led to the lowest extent of thermodynamic irreversibility involved in the process: (1) 550 °C, 0.9 MPa, 200 s, and pure N_2; and (2) 550 °C, 0.9 MPa, 100 s, and CO_2/N_2 60:40 v/v. From a practical point of view, the second set of operating conditions appears to be the most convenient one, since relatively high flow rates of recycled CO_2-containing flue gas could easily be implemented in scaled-up process plants.

4. Conclusions

Despite the fact that there is not a unique combination of pyrolysis operating conditions capable to simultaneously optimize all the response variable analyzed here, some useful considerations can be drawn from the results above discussed:

- Although, as expected, the pyrolysis peak temperature was the most influential operating factor, the absolute pressure also played a key role during the devolatilization process of wheat straw, enhancing the release of the gas species at the expense of the liquid products and without affecting neither the yield of char nor its microporosity. An increased pressure also improved the potential stability of the resulting char, due to the greater extent of the secondary charring reactions. The gas residence time was also responsible to modify the course of the devolatilization, by prolonging the solid/gas phases contact and, consequently, further promoting the secondary char reactions. Its influence was reflected on the improved char yield and carbonization efficiency.
- The switch from a pure N_2 atmosphere to the mixture of CO_2/N_2 resulted to be irrelevant on the pyrolysis behavior of wheat straw pellets, except for a slight increase in the yield of CO released. This finding opens the possibility of recycling the flue gas stream as a gas carrier in the pyrolysis process instead of using a more expensive inert gas. Furthermore, the presence of CO_2 in the carrier gas favored the availability of oxygenated functional groups on the surface of resulting chars, regardless of the peak temperature and absolute pressure.

- From an applied research point of view, the most important finding from this study is the fact that pressurized pyrolysis —which implies a considerable reduction of the reactor vessel as well as the costly downstream compression steps— favors the exergy efficiency of the process, even at relatively high pyrolysis peak temperature. For the biomass feedstock and the range of operating conditions studied here, thermodynamic irreversibilities of the pyrolysis system were considerably lowered when the process was conducted at 550 °C, 0.9 MPa and using a mixture of CO_2 and N_2 as carrier gas at relatively short residence times. Under these same conditions, the resulting produced char also exhibit very good properties in terms of potential stability (which is essential for biochar purposes) as well as a considerable availability of oxygen-containing functionalities on surface with a certain microporosity development (being both properties valuable for further uses of chars in value-added applications).

Acknowledgements

This project has received funding from the European Union's Horizon 2020 research and innovation program under the Marie Skłodowska-Curie grant agreement No 721991. JJM also acknowledge the funding from the Aragón Government (Ref. T22_20R), co-funded by FEDER 2014-2020 "Construyendo Europa desde Aragón".

Appendix A. Supplementary material

Nomenclature

$Area_{peak}$= area of the devolatilization peak (g)

DTG_{max}= peak of the time derivative (g min^{-1})

$e_{out,i}$= exergy of the product *i* (MJ kg^{-1})

h_{in}= input specific enthalpy (MJ kg^{-1})

h_{out}= output specific enthalpy (MJ kg^{-1})

$Q_{process}$ = enthalpy required for the process that should be supplied externally (MJ kg^{-1})

S_{BET} = Brunauer–Emmet–Teller specific surface area (m^2 g^{-1})

TC# = temperatures measured by the thermocouples placed within the reactor (°C)

T_{max} = temperature peak of the devolatilization step (°C)

V_{ultra} = ultra-micropore volume (cm^3 g^{-1})

x_{FC} = mass fraction of fixed-carbon in the char (daf basis)

y_{char} = mass yield of char in a dry and ash-free basis (−)

y_{FC} = fixed-carbon yield in a dry and ash-free basis (−)

y_{gas} = mass yield of produced gas in a dry and ash-free basis (−)

y_{org} = mass yield of condensable organics in a dry and ash-free basis (−)

y_{water} = mass yield of produced water in a dry and ash-free basis (−)

τ = gas residence time

Ψ_{char}= exergy efficiency of the char (−)

Ψ_{gas}= exergy efficiency of the gas product (−)

$\Psi_{process}$= exergy efficiency of the overall process (−)

Σe_{in}= sum of the input exergies (MJ kg^{-1})

Σe_{out}= sum of the output exergies (MJ kg^{-1})

Acronyms

AAEMs = alkali and alkaline Earth metal species

daf = dry-ash-free

FT-IR = Fourier Transform Infrared spectroscopy

GCMC = Grand Canonical Monte Carlo

GHSV = gas hourly space velocity (h^{-1})

HHV = High Heating Value (MJ kg^{-1})

PID = proportional integral derivative

WS = wheat straw

XRF = X-Ray Fluorescence spectroscopy

μ-GC = micro gas chromatograph

References

[1] Lehmann J, Joseph S. Biochar for Environmental Management: An Introduction. Biochar Environ. Manag., Eartschan; 2009, p. 1–10. https://doi.org/10.4324/9780203762264.

[2] Basu P. Biomass Gasification, Pyrolysis and Torrefaction. Burlington: Elsevier Applied Science; 2013. https://doi.org/10.1016/C2011-0-07564-6.

[3] Suhas, Carrott PJM, Ribeiro Carrott MML. Lignin – from natural adsorbent to activated carbon: A review. Bioresour Technol 2007;98:2301–12. https://doi.org/10.1016/J.BIORTECH.2006.08.008.

[4] Mok WS-L, Antal MJ. Effects of pressure on biomass pyrolysis. II. Heats of reaction of cellulose pyrolysis. Thermochim Acta 1983;68:165–86. https://doi.org/10.1016/0040-6031(83)80222-6.

[5] Daugaard DE, Brown RC. Enthalpy for pyrolysis for several types of biomass. Energy and Fuels 2003;17:934–9. https://doi.org/10.1021/ef020260x.

[6] Dincer I, Rosen MA. Exergy: energy, environment and sustainable development. 2nd Editio. Oxford, Great Britain: Elsevier; 2013. https://doi.org/10.1016/B978-0-08-097089-9.00001-2.

[7] Saidur R, BoroumandJazi G, Mekhilef S, Mohammed HA. A review on exergy analysis of biomass based fuels. Renew Sustain Energy Rev 2012;16:1217–22. https://doi.org/https://doi.org/10.1016/j.rser.2011.07.076.

[8] Chaiwatanodom P, Vivanpatarakij S, Assabumrungrat S. Thermodynamic analysis of biomass gasification with CO2 recycle for synthesis gas production. Appl Energy 2014;114:10–7. https://doi.org/https://doi.org/10.1016/j.apenergy.2013.09.052.

[9] Antal MJ, Gronli M. The Art, Science, and Technology of Charcoal Production. Ind Eng Chem Res 2003;42:1619–40. https://doi.org/10.1021/ie0207919.

[10] Duman G, Okutucu C, Ucar S, Stahl R, Yanik J. The slow and fast pyrolysis of cherry seed. Bioresour Technol 2011;102:1869–78. https://doi.org/10.1016/j.biortech.2010.07.051.

[11] Di Blasi C, Signorelli G, Di Russo C, Rea G. Product distribution from pyrolysis of wood and agricultural residues. Ind Eng Chem Res 1999;38:2216–24. https://doi.org/10.1021/ie980711u.

[12] Demirbaş A. Effects of temperature and particle size on bio-char yield from pyrolysis of agricultural residues. J Anal Appl Pyrolysis 2004;72:243–8. https://doi.org/10.1016/j.jaap.2004.07.003.

[13] Antal, M. J. J, Allen SG, Dai X, Shimizu B, Tam MS, Gronli M. Attainment of the Theoretical Yield of Carbon from Biomass. Ind Eng Chem Res 2000;39:4024–31. https://doi.org/10.1021/ie000511u.

[14] Manyà JJ. Pyrolysis for Biochar Purposes: A Review to Establish Current Knowledge Gaps and Research Needs. Environ Sci Technol 2012;46:7939–54. https://doi.org/10.1021/es301029g.

[15] Heo HS, Park HJ, Dong J-I, Park SH, Kim S, Suh DJ, et al. Fast pyrolysis of rice husk under different reaction conditions. J Ind Eng Chem 2010;16:27–31. https://doi.org/10.1016/J.JIEC.2010.01.026.

[16] Akhtar J, Saidina Amin N. A review on operating parameters for optimum liquid oil yield in biomass pyrolysis. Renew Sustain Energy Rev 2012;16:5101–9. https://doi.org/10.1016/J.RSER.2012.05.033.

[17] Guedes RE, Luna AS, Torres AR. Operating parameters for bio-oil production in biomass pyrolysis: A review. J Anal Appl Pyrolysis 2018;129:134–49. https://doi.org/10.1016/J.JAAP.2017.11.019.

[18] Manyà JJ, Alvira D, Azuara M, Bernin D, Hedin N. Effects of Pressure and the Addition of a Rejected Material from Municipal Waste Composting on the Pyrolysis of Two-Phase Olive Mill Waste. Energy & Fuels 2016;30:8055–64. https://doi.org/10.1021/acs.energyfuels.6b01579.

[19] Antal, MJ, Croiset E, Dai X, DeAlmeida C, Mok WS-L, Norberg N, et al. High-Yield Biomass Charcoal †. Energy & Fuels 1996;10:652–8. https://doi.org/10.1021/ef9501859.

[20] Rousset P, Figueiredo C, De Souza M, Quirino W. Pressure effect on the quality of eucalyptus wood charcoal for the steel industry: A statistical analysis approach. Fuel Process Technol 2011;92:1890–7. https://doi.org/10.1016/j.fuproc.2011.05.005.

[21] Recari J, Berrueco C, Abellò S, Montané D, Farriol X. Effect of temperature and pressure on characteristics and reactivity of biomass-derived chars. Bioresour Technol 2014;170:204–10. https://doi.org/10.1016/j.biortech.2014.07.080.

[22] Qian Y, Zhang J, Wang J. Pressurized pyrolysis of rice husk in an inert gas sweeping fixed-bed reactor with a focus on bio-oil deoxygenation. Bioresour Technol 2014;174:95–102. https://doi.org/10.1016/j.biortech.2014.10.012.

[23] Bui H-H, Wang L, Tran K-Q, Skreiberg Ø. CO2 gasification of charcoals produced at various pressures. Fuel Process Technol 2016;152:207–14. https://doi.org/10.1016/J.FUPROC.2016.06.033.

[24] Melligan F, Auccaise R, Novotny EH, Leahy JJ, Hayes MHB, Kwapinski W. Pressurised pyrolysis of Miscanthus using a fixed bed reactor. Bioresour Technol 2011;102:3466–70. https://doi.org/10.1016/j.biortech.2010.10.129.

[25] Manyà JJ, Roca FX, Perales JFJ. TGA study examining the effect of pressure and peak temperature on biochar yield during pyrolysis of two-phase olive mill waste. Anal Appl Pyrolysis 2013;103:86–95. https://doi.org/10.1016/j.jaap.2012.10.006.

[26] Azuara M, Sáiz E, Manso JA, García-Ramos FJ, Manyà JJ. Study on the effects of using a carbon dioxide atmosphere on the properties of vine shoots-derived biochar. Anal Appl Pyrolysis 2017;124:719–25. https://doi.org/10.1016/j.jaap.2016.11.022.

[27] Wang X, Lv W, Guo L, Zhai M, Dong P, Qi G. Energy and exergy analysis of rice husk high-temperature pyrolysis. Int J Hydrogen Energy 2016;41:21121–30. https://doi.org/10.1016/J.IJHYDENE.2016.09.155.

[28] Boateng AA, Mullen CA, Osgood-Jacobs L, Carlson P, Macken N. Mass Balance, Energy, and Exergy Analysis of Bio-Oil Production by Fast Pyrolysis. J Energy Resour Technol 2012;134. https://doi.org/10.1115/1.4007659.

[29] Parvez AM, Wu T, Afzal MT, Mareta S, He T, Zhai M. Conventional and microwave-assisted pyrolysis of gumwood: A comparison study using thermodynamic evaluation and hydrogen production. Fuel Process Technol 2019;184:1–11. https://doi.org/10.1016/J.FUPROC.2018.11.007.

[30] Atienza-Martínez M, Ábrego J, Mastral JF, Ceamanos J, Gea G. Energy and exergy analyses of sewage sludge thermochemical treatment. Energy 2018;144:723–35. https://doi.org/10.1016/J.ENERGY.2017.12.007.

[31] Manyà JJ, Ortigosa MA, Laguarta S, Manso JA. Experimental study on the effect of pyrolysis pressure, peak temperature, and particle size on the potential stability of vine shoots-derived biochar. Fuel 2014;133:163–72. https://doi.org/10.1016/j.fuel.2014.05.019.

[32] Channiwala SA, Parikh PP. A unified correlation for estimating HHV of solid, liquid and gaseous fuels. Fuel 2002;81:1051–63. https://doi.org/10.1016/S0016-2361(01)00131-4.

[33] Montgomery DC. Design and Analysis of Experiments. 6th editio. Hoboken: 2005.

[34] Greco G, Videgain M, Di Stasi C, González B, Manyà JJ. Evolution of the mass-loss rate during atmospheric and pressurized slow pyrolysis of wheat straw in a bench-scale reactor. J Anal Appl Pyrolysis 2018;136:18–26. https://doi.org/10.1016/j.jaap.2018.11.007.

[35] Perry RH, Green DW. Perry's chemical engineers handbook. 7th Editio. Australia: McGraw Hill; 1998.

[36] Szargut J. Exergy method: technical and ecological applications. Outhampton, UK: WIT; 2005.

[37] Zhao L, Cao X, Mašek O, Zimmerman A. Heterogeneity of biochar properties as a function of feedstock sources and production temperatures. J Hazard Mater 2013;256–257:1–9. https://doi.org/10.1016/j.jhazmat.2013.04.015.

[38] McBeath A V., Wurster CM, Bird MI. Influence of feedstock properties and pyrolysis conditions on biochar carbon stability as determined by hydrogen pyrolysis. Biomass Bioenergy 2015;73. https://doi.org/10.1016/j.biombioe.2014.12.022.

[39] Manyà JJ, Laguarta S, Ortigosa MA, Manso JA. Biochar from Slow Pyrolysis of Two-Phase Olive Mill Waste: Effect of Pressure and Peak Temperature on its Potential Stability. Energy & Fuels 2014;28:3271–80. https://doi.org/10.1021/ef500654t.

[40] Noumi ES, Blin J, Valette J, Rousset P. Combined Effect of Pyrolysis Pressure and Temperature on the Yield and CO2 Gasification Reactivity of Acacia Wood in macro-TG. Energy & Fuels 2015;29:7301–8. https://doi.org/10.1021/acs.energyfuels.5b01454.

[41] Ates F, Miskolczi N, Saricaoglu B. Pressurized pyrolysis of dried distillers grains with solubles and canola seed press cake in a fixed-bed reactor. Bioresour Technol 2015;177:149–58. https://doi.org/10.1016/j.biortech.2014.10.163.

[42] Cetin E, Moghtaderi B, Gupta R, Wall T. Influence of pyrolysis conditions on the structure and gasification reactivity of biomass chars. Fuel 2004;83:2139–50. https://doi.org/10.1016/J.FUEL.2004.05.008.

[43] Ding H-S, Jiang H. Self-heating co-pyrolysis of excessive activated sludge with waste biomass: Energy balance and sludge reduction. Bioresour Technol 2013;133:16–22. https://doi.org/10.1016/J.BIORTECH.2013.01.090.

[44] Srinivas T, Gupta AVSSKS, Reddy B V. Thermodynamic equilibrium model and exergy analysis of a Biomass gasifier. J Energy Resour Technol Trans ASME 2009;131:318011–7. https://doi.org/10.1115/1.3185354.

[45] Prins MJ, Ptasinski KJ. Energy and exergy analyses of the oxidation and gasification of carbon. Energy 2005;30:982–1002. https://doi.org/10.1016/J.ENERGY.2004.08.010.